Adaptive Prescribed Performance Non-singular Fast Terminal Backstepping Sliding Mode Control for Quadrotor UAVs with Input Saturation

Xianglong Liu , Zhangsong Shi , Huihui Xu , Hao Wu * , Jialuo Jiang

Posted Date: 19 March 2026

doi: 10.20944/preprints202603.1571.v1

Keywords: quadrotor UAVs; input saturation; prescribed performance function; backstepping; nonsingular fast terminal sliding mode control; RBF neural network

 doi:10.20944/preprints202603.1571.v1

Article

Adaptive Prescribed Performance Non-singular Fast Terminal Backstepping Sliding Mode Control for Quadrotor UAVs with Input Saturation

Xianglong Liu, Zhangsong Shi, Huihui Xu, Hao Wu * and Jialuo Jiang

Naval University of Engineering, Wuhan 430000, China

* Correspondence: 2420241045@nue.edu.cn

Highlights

What are the main findings?

- By defining a new error variable through an offset function and introducing a first-order system into the prescribed performance function, the performance bounds are endowed with a certain adaptive capability with respect to the error dynamics, thereby preventing error violation and avoiding singularity.
- The designed controller and observer are capable of compensating for input saturation and external disturbances, rendering all system state errors uniformly ultimately bounded with minimal chattering.

What are the implications of the main findings?

- This study offers insights and provides a theoretical foundation for the combination of adaptive control and prescribed performance control.
- This research holds positive significance for the advancement of sliding mode control and neural network technologies in the field of quadrotor UAV control.

Abstract

This paper proposes an adaptive prescribed performance sliding mode control method to address the input saturation problem in quadrotor UAVs. An offset function is designed to ensure that the initial values of the system errors always lie within the performance envelope. A first-order system is introduced to analyze error violation and compensate for the performance bounds, thereby enhancing system stability. An anti-windup auxiliary system and a non-singular fast terminal backstepping sliding mode controller are developed to mitigate the adverse effects of input saturation. A piecewise variable rate reaching law is designed to reduce controller chattering. An RBF neural network observer is constructed to compensate online for system modeling uncertainties and external disturbances. The uniform ultimate boundedness of all state errors is rigorously proved using Lyapunov theory. Simulation results demonstrate that, compared to traditional adaptive sliding mode control and PID control, the proposed method reduces the RMSE of the desired trajectory tracking error by 18.5% and 12.9%, respectively, and decreases the IAE by 34.3% and 23.3%, respectively, validating the effectiveness and superiority of the algorithm.

Keywords: quadrotor UAVs; input saturation; prescribed performance function; backstepping; non-singular fast terminal sliding mode control; RBF neural network

1. Introduction

Quadrotor UAVs have garnered extensive attention and application across various industries in recent years due to their low cost, simple structure, flexibility, compact size, strong maneuverability,

 doi:10.20944/preprints202603.1571.v1

and effective stealth capabilities [1]. In the military domain, they are employed for surveillance and reconnaissance [2], precision strikes [3], and material transport [4]; in civilian sectors, their applications include aerial photography [5], environmental monitoring [6], and agricultural production [7]. The realization of these functions invariably depends on the UAV's control system. During flight, a quadrotor exhibits six degrees of freedom, characterizing it as a typical nonlinear, strongly coupled, multi-input multi-output underactuated system. For design convenience, its control system is conventionally partitioned into an inner attitude loop and an outer position loop: the inner loop controls the Euler angles, while the outer loop governs the horizontal position and altitude [8]. However, practical applications must also contend with issues such as modeling uncertainties, external disturbances, rotor failures, input saturation, and communication delays, which significantly complicate the design of the control system [9].

Actuator saturation is a fundamental physical constraint that must be considered in the practical application of quadrotor UAVs. Designing corresponding anti-windup compensation algorithms is a key issue to ensure proper motor operation and safe flight. To address this, the problem of finite-time control for quadrotor systems subject to input saturation and external disturbances was investigated, where an auxiliary system was designed to compensate for saturation effects and a fast terminal sliding mode controller was proposed to achieve trajectory tracking and attitude stabilization [10]. To ensure the stability of quadrotor systems and eliminate the negative effects of input saturation, a saturated adaptive sliding mode control law was developed, integrating the advantages of both sliding mode control and adaptive control [11]. The problem of non-singular finite-time adaptive robust saturated command-filtered control for quadrotors was studied, where saturation compensation signals were designed to suppress the adverse effects of actuator saturation and alleviate control input chattering, thereby satisfying practical finite-time stability requirements [12]. For low-priority yaw-angle flight tasks, an anti-windup controller was proposed to improve thrust allocation efficiency and trajectory tracking performance by prioritizing the thrust demands of the total thrust, roll, and pitch channels before allocating the remaining control authority to the yaw channel [13].

For systems susceptible to disturbances, such as quadrotors, prescribed performance control can achieve high-performance requirements in terms of response time and steady-state accuracy by constraining the errors within a predefined performance envelope. To address this, an improved prescribed performance control strategy was proposed to regulate the transient process of quadrotor trajectory tracking, guaranteeing arbitrarily small overshoot and fast convergence rates even in the presence of triggering errors [14]. By employing backstepping techniques combined with error transformation based on prescribed performance functions, bounded transient and steady-state tracking errors were achieved for the quadrotor system [15]. To eliminate severe transient fluctuations caused by the pursuit of fast convergence in traditional prescribed performance control, a mechanism based on a tracking differentiator was adopted, ensuring that the quadrotor's trajectory states converge to a specified region within a preset time [16]. Addressing the shipboard landing problem for quadrotors, a prescribed performance evolution control method was developed for relative position control to simultaneously guarantee both transient performance and steady-state error during the landing process [17]. Furthermore, a prescribed performance control method incorporating an improved funnel variable was proposed. By embedding a continuous piecewise function to construct the performance envelope, the convergence time can be set independently of initial states and system parameters, constraining the quadrotor's trajectory tracking error curve within the performance bounds without inducing singularities [18].

Sliding mode control (SMC) can rapidly drive system states onto a predefined sliding surface, ultimately converging to the equilibrium point. This mathematical property endows SMC with robust performance when dealing with uncertain dynamical systems such as quadrotors. To this end, a super-twisting terminal sliding mode control method was designed to achieve finite-time attitude and position tracking control for quadrotors subject to input delay, model uncertainties, and wind disturbances [19]. Addressing the issues of model uncertainties and external disturbances, a robust

 doi:10.20944/preprints202603.1571.v1

nonlinear controller integrating sliding mode control and backstepping techniques was proposed. This approach ensures the stability of the closed-loop system by recursively stabilizing each subsystem [20]. For quadrotor attitude and position control under parameter uncertainties and external disturbances, a novel composite controller combining backstepping and fast terminal sliding mode control was developed, with rigorous proofs provided for system stability and robustness against parameter variations [21]. Furthermore, to tackle the trajectory tracking problem of underactuated quadrotors with modeling uncertainties and unknown external disturbances, a new robust nonlinear adaptive controller based on an adaptive non-singular fast terminal sliding mode control algorithm was proposed. This controller ensures finite-time stabilization of the UAV states, avoids the singularity problem, eliminates chattering effects, and exhibits strong robustness against unknown external disturbances and uncertainties [22].

However, despite considerable progress in quadrotor control methodologies, flight performance in practical complex environments remains insufficient—particularly becoming more challenging when simultaneously mitigating the adverse effects of unknown disturbances and input saturation while ensuring satisfactory response metrics. To address these issues, this paper proposes a more adaptive and robust control method building upon existing research findings. The main contributions are as follows:

- An adaptive prescribed performance sliding mode control method is proposed for quadrotor UAVs subject to modeling uncertainties, external disturbances, and input saturation, ensuring the uniform ultimate boundedness of all state errors.
- An offset function is designed to redefine the error variables, ensuring that the initial system errors remain within the prescribed performance envelope from the initial moment. A first-order system is introduced to analyze potential error violations and compensate for the performance bounds; when errors are at risk of violating the constraints, this mechanism relaxes the performance bounds, enhancing system stability.
- An anti-windup auxiliary system and a non-singular fast terminal backstepping sliding mode controller are designed to eliminate the adverse effects of input saturation. A piecewise variable rate reaching law is developed to reduce controller chattering. An RBF neural network observer is constructed to compensate online for system modeling uncertainties and external disturbances.

The structure of this paper is organized as follows: Section 2 presents the six-degree-of-freedom dynamic model of the quadrotor UAV. Section 3 details the control system design and the corresponding stability proof. In Section 4, a comparative and quantitative analysis of simulation results is presented to validate the effectiveness of the proposed controller and demonstrate its superiority over traditional methods. Finally, Section 5 concludes the paper by summarizing the research and presenting the key findings.

2. Quadrotor Mathematical Model

The dynamic model of a quadrotor subject to external disturbances and input saturation is given by [23]:

 doi:10.20944/preprints202603.1571.v1

$$\begin{cases} \ddot{x} = \dfrac{sat(U_1)}{m}(\cos\phi\sin\theta\cos\psi + \sin\phi\sin\psi) + d_x \\ \ddot{y} = \dfrac{sat(U_1)}{m}(\cos\phi\sin\theta\sin\psi - \sin\phi\cos\psi) + d_y \\ \ddot{z} = \dfrac{sat(U_1)}{m}\cos\phi\cos\theta - g + d_z \\ \ddot{\phi} = \dfrac{I_y - I_z}{I_x}\dot{\theta}\dot{\psi} + \dfrac{1}{I_x}sat(U_\phi) + d_\phi \\ \ddot{\theta} = \dfrac{I_z - I_x}{I_y}\dot{\phi}\dot{\psi} + \dfrac{1}{I_y}sat(U_\theta) + d_\theta \\ \ddot{\psi} = \dfrac{I_x - I_y}{I_z}\dot{\theta}\dot{\phi} + \dfrac{1}{I_z}sat(U_\psi) + d_\psi \end{cases} \tag{1}$$

where $[x\ y\ z\ \phi\ \theta\ \psi]^T$ denotes the six-degree-of-freedom (DOF) state variables, $sat(\cdot)$ is the saturation function, U_i represents the desired control input, and $sat(U_i)$ is the actual control input $(i = 1, \phi, \theta, \psi)$.

The expression of the saturation function is given as follows:

$$sat(U) = \begin{cases} \bar{U}, & U > \bar{U} \\ U, & \underline{U} \le U \le \bar{U} \\ \underline{U}, & U < \underline{U} \end{cases} \tag{2}$$

where $\bar{U} > 0$ and $\underline{U} < 0$ are the set maximum and minimum values of the control input, respectively.

The quadrotor dynamic model (1) is transformed into the state-space form:

$$\begin{cases} \dot{x}_1 = x_2 \\ \dot{x}_2 = Gu_{sat} + f(x) + d \end{cases} \tag{3}$$

where $x_1 = [x, y, z, \phi, \theta, \psi]^T$, $x_2 = [\dot{x}, \dot{y}, \dot{z}, \dot{\phi}, \dot{\theta}, \dot{\psi}]^T$, $G = diag\left[\frac{1}{m}, \frac{1}{m}, \frac{1}{m}, \frac{1}{I_x}, \frac{1}{I_y}, \frac{1}{I_z}\right]$,

$u_{sat} = [sat(U_x), sat(U_y), sat(U_z), sat(U_\phi), sat(U_\theta), sat(U_\psi)]^T$, $d = [d_x, d_y, d_z, d_\phi, d_\theta, d_\psi]^T$,

$sat(U_x) = sat(U_1)(\cos\phi\sin\theta\cos\psi + \sin\phi\sin\psi)$, $U_x = U_1(\cos\phi_d\sin\theta_d\cos\psi_d + \sin\phi_d\sin\psi_d)$,

$sat(U_y) = sat(U_1)(\cos\phi\sin\theta\sin\psi - \sin\phi\cos\psi)$, $U_y = U_1(\cos\phi_d\sin\theta_d\sin\psi_d - \sin\phi_d\cos\psi_d)$,

$sat(U_z) = sat(U_1)\cos\phi\cos\theta$, $U_z = U_1\cos\phi_d\cos\theta_d$, $f(x) = \left[0, 0, -g, \frac{I_y - I_z}{I_x}\dot{\theta}\dot{\psi}, \frac{I_z - I_x}{I_y}\dot{\phi}\dot{\psi}, \frac{I_x - I_y}{I_z}\dot{\phi}\dot{\theta}\right]^T$.

Combining equation (1), equation (3), and the desired yaw angle ψ_d, we obtain:

$$\begin{cases} \theta_d = \arctan\left(\dfrac{U_x\cos\psi_d + U_y\sin\psi_d}{U_z}\right) \\ \phi_d = \arctan\left[\dfrac{\cos\theta_d(U_x\sin\psi_d + U_y\cos\psi_d)}{U_z}\right] \\ U_1 = \dfrac{U_z}{\cos\theta_d\cos\phi_d} \end{cases} \tag{4}$$

For the purpose of focusing on the core problem and facilitating the controller design, the following reasonable assumptions are given:

 doi:10.20944/preprints202603.1571.v1

Assumption 1 ([24]). The desired trajectory signals x_d, y_d, z_d, ψ_d are continuous and bounded, and their first and second derivatives exist.

Assumption 2 ([25]). The system disturbance d is continuous and bounded, and varies slowly.

Assumption 3 ([26]). The optimal parameters of the observer are bounded, and the approximation error for the disturbance d is bounded.

3. Control System Design

3.1. PPF Design and Error Transformation

Define the actual tracking error as

$$e_1 = x_1 - x_{1\mathrm{d}} \tag{5}$$

where $x_{1\mathrm{d}} = \left[x_{\mathrm{d}}, y_{\mathrm{d}}, z_{\mathrm{d}}, \mathrm{f}_{\mathrm{d}}, \theta_{\mathrm{d}}, \psi_{\mathrm{d}}\right]^{\mathrm{T}}$ denotes the desired position and attitude of the quadrotor, and $e_1 = \left[e_x, e_y, e_z, e_{\mathrm{f}}, e_\theta, e_\psi\right]^{\mathrm{T}}$ represents the actual tracking errors of the six states.

Define a new error variable as

$$e_n(t) = e_1(t) - e_1(0)\beta(t) \tag{6}$$

$$\beta(t) = \begin{cases} \left[1 - \tanh\left(\dfrac{t}{T_s - t}\right)\right] \mathrm{e}^{\frac{t}{t - T_s}}, & 0 \le t < T_s \\ 0, & t \ge T_s \end{cases} \tag{7}$$

where $\beta(t)$ is an offset function designed to ensure that the error does not violate the bounds at the initial moment.

The prescribed performance function is designed as follows:

$$\rho(t) = (\rho_0 - \rho_\infty)\beta(t) + \rho_\infty + \rho_c(t) \tag{8}$$

$$\dot{\rho}_c = \frac{C_1}{1-b}(-\rho_c + \rho_{c1}) \tag{9}$$

$$\rho_{c1} = \begin{cases} \dfrac{C_2}{1-b}\left|sat(b) - b\right|(\dot{e}_n - \dot{\rho}), & e_n > 0, \dot{e}_n > \dot{\rho} \\ \dfrac{C_2}{1-b}\left|sat(b) - b\right|(-\dot{\rho} - \dot{e}_n), & e_n < 0, \dot{e}_n < -\dot{\rho} \\ 0, & else \end{cases} \tag{10}$$

where $\rho_0 > \rho_\infty > 0$, $C_1, C_2 > 0$, $\bar{b} = 0.5$, $\underline{b} = -0.5$ .where $\rho_c(t)$ is a compensation term designed to widen the performance bounds in the event of potential error violation at non-initial moments.

The error is further transformed as

$$\begin{cases} b = \dfrac{e_n(t)}{\rho(t)} \\ e_\rho(t) = \dfrac{1}{2}\ln\left(\dfrac{1+b}{1-b}\right) \end{cases} \tag{11}$$

 doi:10.20944/preprints202603.1571.v1

Through the transformation above and the proof of the stability of e_ρ, the condition $-\rho(t) < e_n(t) < \rho(t)$ can be achieved, thereby realizing the performance constraints of $e_1(0)\beta(t) - \rho(t) < e_1(t) < e_1(0)\beta(t) + \rho(t)$.

It can be further deduced that

$$\begin{gathered} -\rho(t) < e_1(t) - e_1(0)\beta(t) < \rho(t) \\ \Downarrow \\ e_1(0)\beta(t) - \rho(t) < e_1(t) < e_1(0)\beta(t) + \rho(t) \\ \Downarrow t = 0 \\ e_1(0) - \rho_0 < e_1(0) < e_1(0) + \rho_0 \end{gathered} \tag{12}$$

Since the above equation holds true, it follows that $e_1(0)$ will never exceed the prescribed bounds.

Taking the time derivative of e_ρ in Equation (12) yields

$$\dot{e}_\rho = a(\dot{e}_n - c) \tag{13}$$

where $a = \frac{1}{2\rho}\left(\frac{1}{1+b} + \frac{1}{1-b}\right) > 0$, $c = \frac{e_n\dot{\rho}}{\rho}$.

Taking the derivative again yields

$$\ddot{e}_\rho = a(\ddot{e}_n - \dot{c}) + \dot{a}(\dot{e}_n - c) \tag{14}$$

where $\dot{a} = -\frac{\dot{\rho}}{2\rho^2}\left(\frac{1}{1+b} + \frac{1}{1-b}\right) - \frac{\dot{b}}{2\rho}\left(\frac{1}{(1+b)^2} - \frac{1}{(1-b)^2}\right)$, $\dot{c} = \frac{\dot{e}_n\dot{\rho} + e_n\ddot{\rho}}{\rho} - \frac{e_n\dot{\rho}^2}{\rho^2}$.

3.2. RBFNN Observer Design

An RBF neural network observer is constructed in this paper to estimate and compensate for unknown disturbances. Let $x_r = [x_{r1}, x_{r2}, \cdots, x_{rm}]^{\mathrm{T}}$ be the input vector to the neural network, $h_r = [h_{r1}, h_{r2}, \cdots, h_{rm}]^{\mathrm{T}}$ denote the output of the hidden layer, and $w_r = [w_{r1}, w_{r2}, \cdots, w_{rm}]^{\mathrm{T}}$ represent the weight of the hidden layer output. Specifically, h_{rj} is computed by Gaussian basis functions as follows:

$$h_{rj} = \exp\left(-\frac{\|x_r - c_{rj}\|^2}{2b_{rj}^2}\right), j = (1, 2, \cdots, m) \tag{15}$$

The ideal output of the neural network is

$$d = w_r^{*T} h_r + e_{RBF} \tag{16}$$

where w_{rj}^* is the optimal parameter vector of w_{rj}, and e_{RBF} denotes the approximation error between the network's estimate and the actual value.

Since the optimal parameters are unavailable, the actual output is given by:

$$\hat{d} = \hat{w}_r^T h_r + \hat{e}_{RBF} \tag{17}$$

where $\hat{w}_{rj}$ is the estimate of w_{rj}^*, and $\hat{e}_{RBF}$ is the estimate of e_{RBF}, which is designed as:

$$\hat{e}_{RBF} = \hat{\lambda}\tanh(\mu s) \tag{18}$$

where $\hat{\lambda}$ is the estimate of the optimal parameter λ^*, $\mu > 0$.

 doi:10.20944/preprints202603.1571.v1

The online learning of the neural network is implemented via equation (32).

3.3. Auxiliary System Design

The anti-windup auxiliary system is designed as follows:

$$\dot{\xi} = -k_{\xi}\xi + \Delta u \tag{19}$$

where $k_{\xi} > 0$, $\Delta u = u_{sat} - u_d$, $u_d = \left[U_{xd}, U_{yd}, U_{zd}, U_{\mathrm{f}}, U_{\theta}, U_{\psi}\right]^T$.

3.4. Reaching Law Design

The robustness of sliding mode variable structure control for uncertain dynamic systems derives from the inclusion of a discontinuous sign function $\mathrm{sgn}(\cdot)$ in the controller, which continuously adapts the control structure according to the system state. However, this mathematical characteristic inevitably causes the system state to chatter across the sliding surface, leading to undesirable chattering phenomena. In severe cases, such chattering may excite high-frequency system dynamics, compromise system stability, and degrade controller performance. In light of this, a piecewise variable rate reaching law is designed in this paper. Compared to traditional methods, the novel parameters can adaptively adjust according to the system state, thereby effectively mitigating chattering:

$$\begin{cases} \dot{s}_1 = -\dfrac{lr}{n^{1-\Delta}}s - \dfrac{v}{r}\chi(s)\mathrm{sgn}(s) \\ r = \delta + (1-\delta)\mathrm{e}^{-\varepsilon|s|^{\gamma}} \end{cases} \tag{20}$$

$$\chi(s) = \begin{cases} 1, |s| \geq n \\ \left|\dfrac{s}{n}\right|^{\frac{n}{\Delta}}, |s| < n \end{cases} \tag{21}$$

where $l, v, \varepsilon, \gamma > 0$, $0 < \delta < 1$, $0 < \Delta < n < 1$, $\chi(s)$ is a piecewise function.

When the error approaches the sliding surface, $|s|$ decreases, while $\mathrm{e}^{-\varepsilon|s|^{\gamma}}$ and r increase. Consequently, the switching gain $\dfrac{v}{r}$ decreases, effectively suppressing chattering near the sliding surface. Conversely, when the error is far from the sliding surface, $|s|$ increases while $\mathrm{e}^{-\varepsilon|s|^{\gamma}}$ and r decrease. This results in an increased switching gain $\dfrac{v}{r}$, accelerating the error convergence rate.

3.5. Sliding Mode Controller Design

The Lyapunov function for the error is designed as:

$$V_{c1} = \frac{1}{2}e_{\rho}^{T}e_{\rho} \tag{22}$$

Taking the derivative of the above Lyapunov function yields:

$$\begin{aligned} \dot{V}_{c1} &= e_{\rho}a\left(\dot{e}_n - c\right) = e_{\rho}a\left(\dot{e}_1 - e_1(0)\dot{\beta}(t) - c\right) \\ &= e_{\rho}a\left(\dot{x}_1 - \dot{x}_{1d} - e_1(0)\dot{\beta}(t) - c\right) = e_{\rho}a\left(x_2 - \dot{x}_{1d} - e_1(0)\dot{\beta}(t) - c\right) \end{aligned} \tag{23}$$

Based on the above equation, the intermediate virtual control law is designed as:

$$e_2 = x_2 - \dot{x}_{1d} - e_1(0)\dot{\beta}(t) - c + \eta e_{\rho} \tag{24}$$

 doi:10.20944/preprints202603.1571.v1

where $\eta > 0$.

The non-singular fast terminal sliding mode surface is designed as:

$$s = k_{s1} \ln\left[k_{s2} \cosh\left(e_\rho^{\frac{p}{q}}\right)\right] \tanh(k_{s3} e_\rho) + e_2 + k_{s4}\xi = \Gamma + e_2 + k_{s4}\xi \tag{25}$$

where $s = \left[s_x, s_y, s_z, s_f, s_\theta, s_\psi\right]^{\mathrm{T}}$ denotes the sliding mode surfaces corresponding to the six degrees of freedom, $k_{s1}, k_{s3}, k_{s4} > 0$, $k_{s2} > 1$, $\frac{1}{2} < \frac{p}{q} < 1$, p and q are coprime positive odd integers..

Taking the derivative of the above equation yields:

$$\begin{aligned} \dot{s}_2 &= k_{s1}\frac{p}{q}\tanh\left(e_\rho^{\frac{p}{q}}\right)e_\rho^{\frac{p}{q}-1}\dot{e}_\rho \tanh(k_{s3}e_\rho) + k_{s1}\ln\left[k_{s2}\cosh\left(e_\rho^{\frac{p}{q}}\right)\right] \\ &* k_{s3}\left(1-\tanh^2(k_{s3}e_\rho)\right)\dot{e}_\rho + \dot{e}_2 + k_{s4}\dot{\xi} = \dot{\Gamma} + \dot{e}_2 + k_{s4}\dot{\xi} \end{aligned} \tag{26}$$

Since $e_\rho \to 0$ and $\tanh e_\rho \sim e_\rho$, we obtain:

$$\lim_{e_\rho \to 0} k_{s1}\frac{p}{q}\tanh\left(e_\rho^{\frac{p}{q}}\right)e_\rho^{\frac{p}{q}-1}\dot{e}_\rho \tanh(k_{s3}e_\rho) = \lim_{e_\rho \to 0} k_{s1}k_{s3}\frac{p}{q}e_\rho^{\frac{2p}{q}}\dot{e}_\rho = 0 \tag{27}$$

Therefore, $\dot{s}_2$ is continuous at $e_\rho = 0$ and possesses $k_{s1}\frac{p}{q}\tanh\left(e_\rho^{\frac{p}{q}}\right)e_\rho^{\frac{p}{q}-1}\dot{e}_\rho \tanh(k_{s3}e_\rho) = 0$; consequently, s is continuously differentiable over the entire domain, ensuring non-singularity.

The Lyapunov function for the controller is designed as:

$$V_c = V_{c1} + \frac{1}{2}\xi^T\xi + \frac{1}{2}s^T s + \frac{1}{2\sigma_1}\tilde{w}_r^T\tilde{w}_r + \frac{1}{2\sigma_2}\tilde{\lambda}^T\tilde{\lambda} \tag{28}$$

where $\tilde{w}_r = w_r^* - \hat{w}_r$, $\tilde{\lambda} = \lambda^* - \hat{\lambda}$, $\sigma_1, \sigma_2 > 0$.

Taking the derivative of the above Lyapunov function yields:

$$\begin{aligned} \dot{V}_c &= \dot{V}_{c1} + \xi\dot{\xi} + s(\dot{\Gamma} + \dot{e}_2 + k_{s4}\dot{\xi}) - \frac{1}{\sigma_1}\tilde{w}_r^T\dot{\hat{w}}_r - \frac{1}{\sigma_2}\tilde{\lambda}^T\dot{\hat{\lambda}} \\ &= \dot{V}_{c1} + \xi\dot{\xi} + s[\dot{\Gamma} + Gu_{sat} + f(x) + d - \ddot{x}_{1\mathrm{d}} - e_1(0)\ddot{\beta}(t) - \dot{c} + \eta\dot{e}_\rho + k_{s4}\dot{\xi}] \\ &\quad -\frac{1}{\sigma_1}\tilde{w}_r^T\dot{\hat{w}}_r - \frac{1}{\sigma_2}\tilde{\lambda}^T\dot{\hat{\lambda}} \\ &= e_\rho a\left(e_2 - \eta e_\rho\right) + \xi(-k_\xi\xi + \Delta u) + s[\dot{\Gamma} + G(u_d + \Delta u) + f(x) + d \\ &\quad -\ddot{x}_{1\mathrm{d}} - e_1(0)\ddot{\beta}(t) - \dot{c} + \eta\dot{e}_\rho + k_{s4}(-k_\xi\xi + \Delta u)] - \frac{1}{\sigma_1}\tilde{w}_r^T\dot{\hat{w}}_r - \frac{1}{\sigma_2}\tilde{\lambda}^T\dot{\hat{\lambda}} \\ &= ae_\rho e_2 - a\eta e_\rho^2 + (\Gamma + e_2 + k_{s4}\xi)[\dot{\Gamma} + Gu_d + f(x) + d - \ddot{x}_{1\mathrm{d}} - e_1(0)\ddot{\beta}(t) \\ &\quad -\dot{c} + \eta\dot{e}_\rho - k_{s4}k_\xi\xi] - k_\xi\xi^2 + [\xi + (G + k_{s4})s]\Delta u - \frac{1}{\sigma_1}\tilde{w}_r^T\dot{\hat{w}}_r - \frac{1}{\sigma_2}\tilde{\lambda}^T\dot{\hat{\lambda}} \end{aligned} \tag{29}$$

The controller u_d is designed as follows:

$$u_d = \frac{1}{G}[-ae_\rho - \dot{\Gamma} - f(x) - \hat{d} + \ddot{x}_{1\mathrm{d}} + e_1(0)\ddot{\beta}(t) + \dot{c} - \eta\dot{e}_\rho + k_{s4}k_\xi\xi + \dot{s}_1] \tag{30}$$

 doi:10.20944/preprints202603.1571.v1

3.6. Stability Proof

Substituting equation (30) into (29) yields:

$$\begin{aligned}\dot{V}_c = &-ae_\rho(\Gamma + k_{s4}\xi) - a\eta\left\|e_\rho\right\|^2 - \frac{lr}{n^{1-\Delta}}s^2 - \frac{v}{r}\chi(s)|s| - k_\xi\left\|\xi\right\|^2 + \\ &[\xi + (G+k_{s4})s]\Delta u + \tilde{w}_r^T(sh_r - \frac{1}{\sigma_1}\dot{\hat{w}}_r) + \tilde{\lambda}^T[s\tanh(\mu s) - \frac{1}{\sigma_2}\dot{\hat{\lambda}}]\end{aligned} \tag{31}$$

The adaptive update law for the neural network is designed as:

$$\begin{cases}\dot{\hat{w}}_r = \sigma_1(sh_r - \hat{w}_r) \\ \dot{\hat{\lambda}} = \sigma_2[s\tanh(\mu s) - \hat{\lambda}]\end{cases} \tag{32}$$

From equation (31), it can be further derived that:

$$\begin{aligned}\dot{V}_c &\le -ae_\rho\Gamma - ak_{s4}e_\rho\xi - a\eta\left\|e_\rho\right\|^2 - \frac{lr}{n^{1-\Delta}}s^2 \\ &\quad +[\xi + (G+k_{s4})s]\Delta u + \tilde{w}_r^T\hat{w}_r + \tilde{\lambda}^T\hat{\lambda} \\ &\le -ae_\rho\Gamma + ak_{s4}\left\|e_\rho\right\|\left\|\xi\right\| - a\eta\left\|e_\rho\right\|^2 - \frac{lr}{n^{1-\Delta}}s^2 + \xi\Delta u \\ &\quad +(G+k_{s4})s\Delta u - \frac{1}{2}\left\|\tilde{w}_r\right\|^2 - \frac{1}{2}\left\|\tilde{\lambda}\right\|^2 + \frac{1}{2}\left\|w_r^*\right\|^2 + \frac{1}{2}\left\|\lambda^*\right\|^2\end{aligned} \tag{33}$$

Since $k_{s2}\cosh\left(e_\rho^{\frac{p}{q}}\right) \ge 1$, it follows that $k_{s1}\ln\left[k_{s2}\cosh\left(e_\rho^{\frac{p}{q}}\right)\right] \ge 0$ and $e_\rho\tanh(k_{s3}e_\rho) \ge 0$, and consequently $ae_\rho[k_{s1}\ln(k_{s2}\cosh\left(e_\rho^{\frac{p}{q}}\right))\tanh(k_{s3}e_\rho)] \ge 0$. Let $\frac{lr}{n^{1-\Delta}} = A$. From the above equation, it can be further derived that:

$$\begin{aligned}\dot{V}_c &\le \frac{ak_{s4}}{2}(\left\|e_\rho\right\|^2 + \left\|\xi\right\|^2) - a\eta\left\|e_\rho\right\|^2 + \frac{1}{2}\left\|s\right\|^2 - A\left\|s\right\|^2 + \frac{1}{2}(\left\|\xi\right\|^2 + \left\|\Delta u\right\|^2) \\ &\quad + \frac{G+k_{s4}}{2}(\left\|s\right\|^2 + \left\|\Delta u\right\|^2) - \frac{1}{2}\left\|\tilde{w}_r\right\|^2 - \frac{1}{2}\left\|\tilde{\lambda}\right\|^2 + \frac{1}{2}\left\|w_r^*\right\|^2 + \frac{1}{2}\left\|\lambda^*\right\|^2 \\ &\le -\frac{a(2\eta - k_{s4})}{2}\left\|e_\rho\right\|^2 - \frac{2A-1-G-k_{s4}}{2}\left\|s\right\|^2 - \frac{1}{2}\left\|\tilde{w}_r\right\|^2 - \frac{1}{2}\left\|\tilde{\lambda}\right\|^2 \\ &\quad + \frac{ak_{s4}+1}{2}\left\|\xi\right\|^2 + \frac{G+k_{s4}+1}{2}\left\|\Delta u\right\|^2 + \frac{1}{2}\left\|w_r^*\right\|^2 + \frac{1}{2}\left\|\lambda^*\right\|^2\end{aligned} \tag{34}$$

Take

$$\begin{cases}2\eta - k_{s4} > 0 \\ 2A - 1 - G - k_{s4} > 0\end{cases} \tag{35}$$

we obtain $0 < k_{s4} < \min(2\eta, 2A - G - 1)$.

From equation (34), it can be further derived that:

$$\begin{aligned}\dot{V}_c &\le -K_C V_c + \frac{ak_{s4}+1+K_C}{2}\left\|\xi\right\|^2 \\ &\quad + \frac{G+k_{s4}+1}{2}\left\|\Delta u\right\|^2 + \frac{1}{2}\left\|w_r^*\right\|^2 + \frac{1}{2}\left\|\lambda^*\right\|^2 \\ &\le -K_C V_c + \Omega\end{aligned} \tag{36}$$

where $K_C = \min\{a(2\eta - k_{s4}), 2A - 1 - G - k_{s4}, 1\} > 0$, Ω is the sum of all bounded terms..

Thus, the uniform ultimate boundedness of all system states is proven.

 doi:10.20944/preprints202603.1571.v1

4. Simulation Verification

The proposed control method is validated through simulations conducted on a quadrotor platform developed in Matlab/Simulink. The dynamic and controller parameters of the quadrotor are set as: $m = 2kg$, $L = 0.2m$, $g = 9.8m/s^2$, $I_x = I_y = 0.002kg \cdot m^2$, $I_z = 0.004kg \cdot m^2$, $\bar{U}_1 = 20$, $\underline{U}_1 = -20$, $\bar{U}_\phi = 2$, $\underline{U}_\phi = -2$, $\bar{U}_\theta = 2$, $\underline{U}_\theta = -2$, $\bar{U}_\psi = 2$, $\underline{U}_\psi = -2$, $k_\xi = 1$, $C_1 = 0.5$, $\mu = 10$, $l = 2$, $n = 0.4$, $\Delta = 0.01$, $\upsilon = 0.1$, $\delta = 0.5$, $\varepsilon = 10$, $\gamma = 1.5$, $k_{s1} = 0.1$, $k_{s2} = 3$, $k_{s3} = 5$, $k_{s4} = 1$, $p = 5$, $q = 9$, $\sigma_1 = 1$, $\sigma_2 = 1$, $\rho_0 = [1, 0.6, 0.6, 0.2, 0.6, 0.6]^T$, $\rho_\infty = [0.05, 0.05, 0.05, 0.02, 0.02, 0.02]^T$, $\eta = [2, 2, 2, 1, 1, 10]^T$.

The initial position, desired trajectory, and time-varying disturbances for the simulation are set as follows:

$$[x_0, y_0, z_0, \phi_0, \theta_0, \psi_0]^T = [0, 0, 0, 0, 0, 0]^T$$

$$[x_d, y_d, z_d, \psi_d]^T = [\sin t + 0.5, \cos t - 0.5, t + 0.5, 0]^T$$

$$d_i = \begin{cases} 0.2\cos t, & t < \dfrac{3\pi}{2} \\ 0.5(\cos t + \sin 2t), & t \geq \dfrac{3\pi}{2} \end{cases}, i = (x, y, z, \phi, \theta, \psi)$$

To validate the effectiveness and superiority of the proposed controller, a comparative analysis is conducted between the control algorithm developed in this paper (denoted as "PPASMC") and traditional adaptive sliding mode control (ASMC) as well as adaptive PID control (APID). The error convergence processes are compared, with PPF denoting the prescribed performance bounds. By selecting appropriate error indices, the tracking data of each desired degree-of-freedom trajectory under different methods are quantitatively compared.

To facilitate a comprehensive performance evaluation and comparison, the root mean square error (RMSE) and the integral of absolute error (IAE) are employed to quantitatively analyze the tracking response process.

$$RMSE = \sqrt{\frac{1}{n}\sum_{i=1}^{n}(y - y_d)^2} \tag{37}$$

$$IAE = \int |e(t)| dt \tag{38}$$

where y denotes the actual value, y_d denotes the desired value, and n is the number of samples, $e = y - y_d$.

As illustrated in Figures 1 and 2, in the presence of external disturbances and input saturation, the PPASMC, ASMC, and APID controllers enable the quadrotor to attain position tracking within 1.5 s, 2.5 s, and 2 s, respectively, while completing attitude adjustment within 1 s, 3 s, and 2.5 s. The proposed PPASMC exhibits superior rapidity and robustness, consistently maintaining tracking response errors within the prescribed performance envelope, achieving high convergence accuracy, and realizing a faster convergence rate in the inner attitude loop compared to the outer position loop, thereby further enhancing system stability. In contrast, both ASMC and APID demonstrate inferior rapidity and robustness, lower convergence accuracy, and suffer from error violation issues, which compromise system stability.

 doi:10.20944/preprints202603.1571.v1

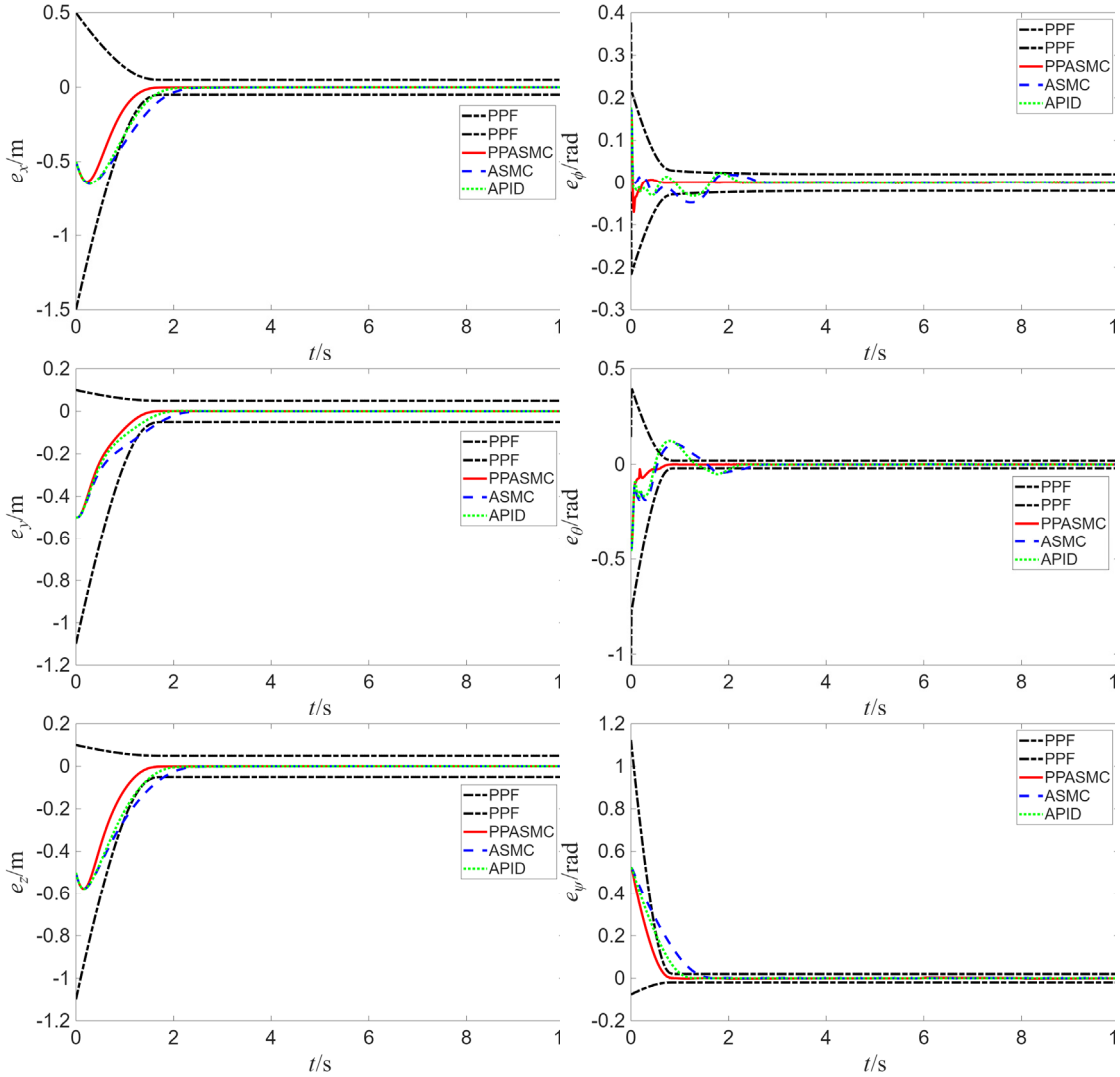

(**a**) Position loop tracking error (**b**) Attitude loop tracking error

Figure 1. Six-degree-of-freedom tracking error.

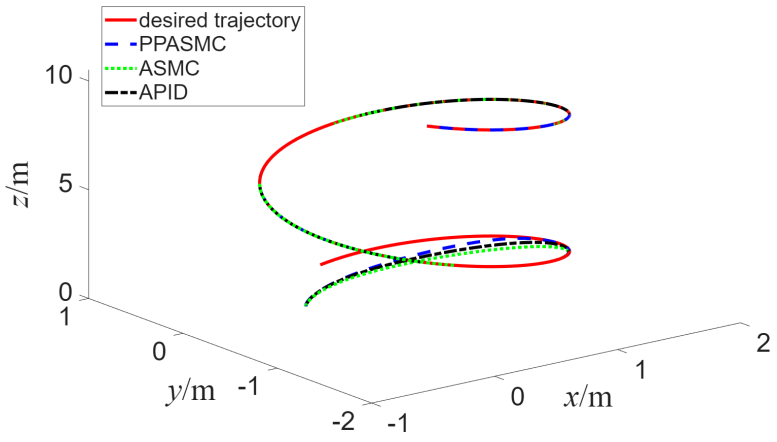

Figure 2. Trajectory tracking performance.

As presented in Tables 1 and 2, compared to ASMC and APID, the proposed PPASMC reduces the RMSE by 18.5% and 12.9%, respectively, and decreases the IAE by 34.3% and 23.3%, respectively.

 doi:10.20944/preprints202603.1571.v1

The results demonstrate that the proposed method achieves shorter convergence time, higher control accuracy, and enhanced robustness.

Table 1. The RMSE calculation results.

Controller	RMSE				Average
	x	y	z	ψ	
PPASMC	0.1507	0.0957	0.1284	0.0729	0.1119
ASMC	0.1885	0.1082	0.1508	0.1017	0.1373
APID	0.1799	0.1002	0.1449	0.0887	0.1284

Table 2. The IAE calculation results.

Controller	IAE				Average
	x	y	z	ψ	
PPASMC	0.4772	0.2874	0.3977	0.1707	0.3332
ASMC	0.7394	0.4002	0.5697	0.3206	0.5075
APID	0.6599	0.3295	0.5095	0.2381	0.4343

As shown in Figure 3, the controller design proposed in this paper takes into account practical application considerations. To mitigate the adverse effects of input saturation on the actuators, amplitude limiting is applied to all four control inputs of the quadrotor. Furthermore, the designed piecewise variable rate reaching law effectively attenuates chattering, thereby enhancing the applicability of the algorithm. This contributes to prolonged motor endurance and ensures safe flight of the UAV.

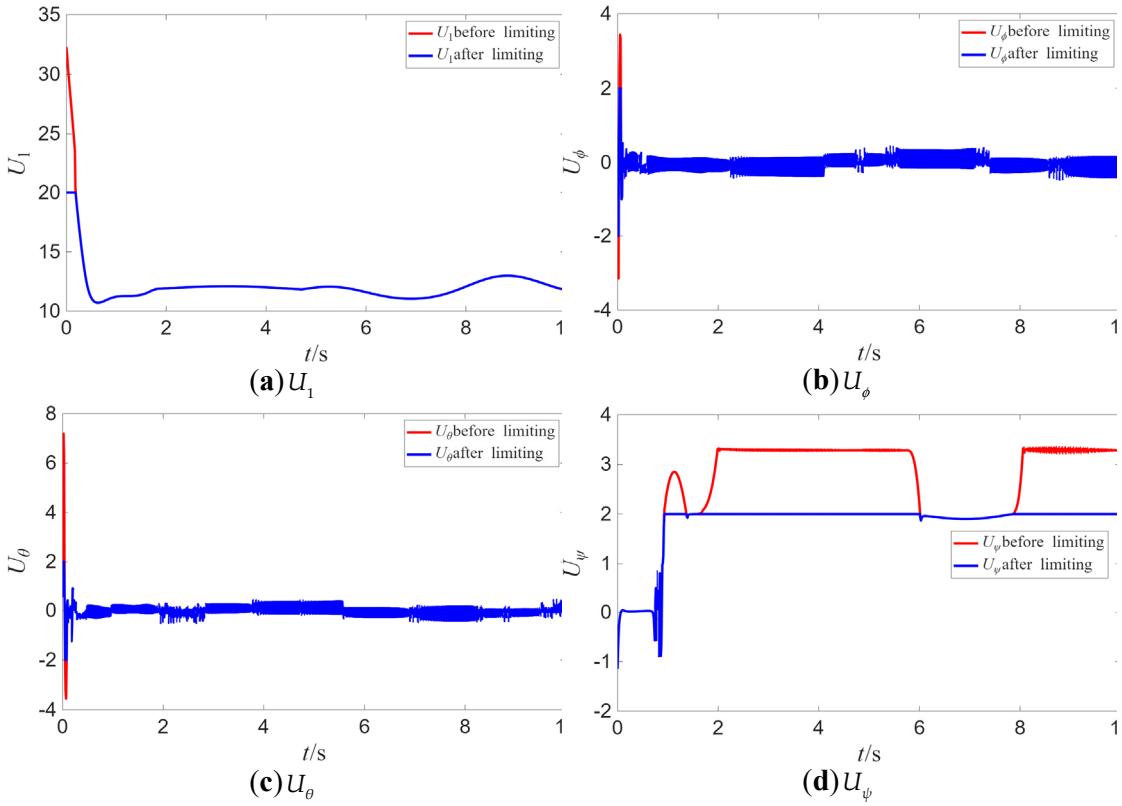

Figure 3. Controller output.

As illustrated in Figure 4, the neural network observer proposed in this paper is capable of updating parameters online and achieving relatively accurate estimation of slowly varying

 doi:10.20944/preprints202603.1571.v1

disturbances, while ensuring that the estimation errors of both the optimal parameters and the disturbances remain bounded.

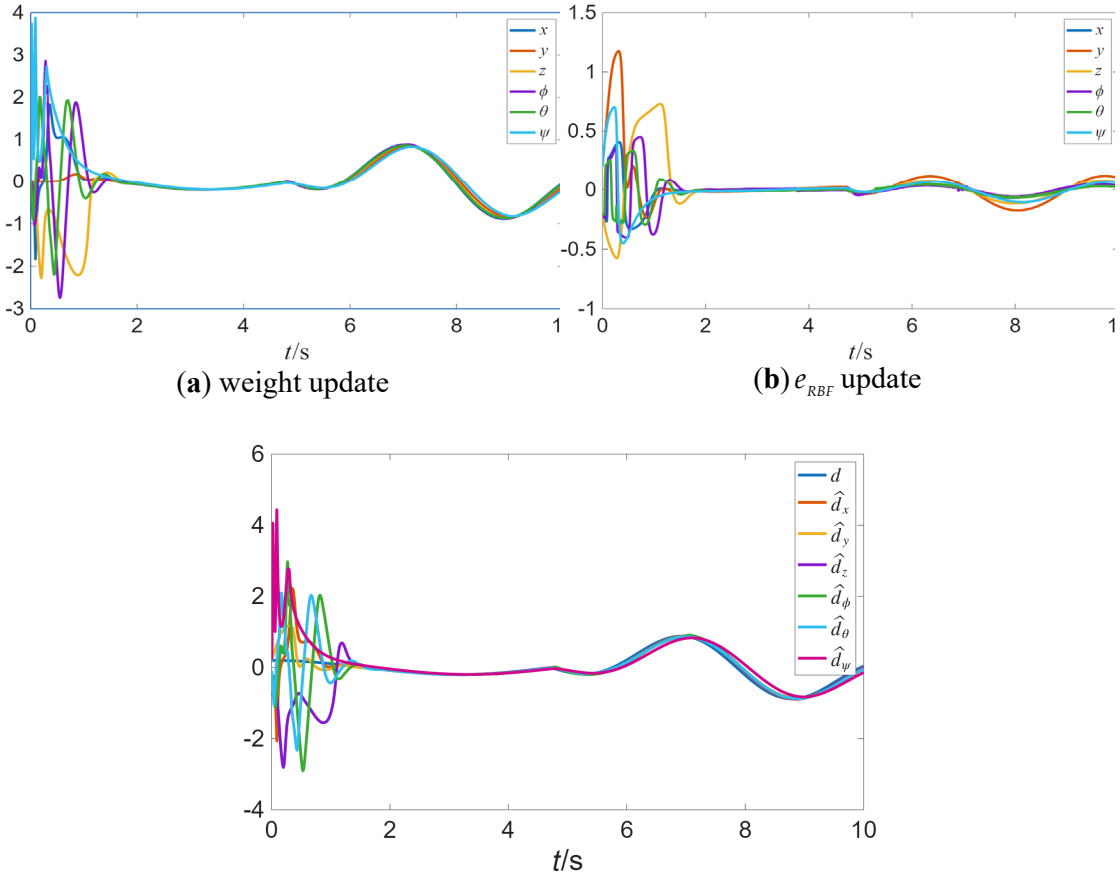

(**a**) weight update (**b**) e_{RBF} update

(**c**) Time-varying disturbance estimation

Figure 4. Disturbance estimation via RBFNN observer.

As shown in Figure 5, the first-order compensation system designed in this paper is capable of predicting potential error violations to a certain extent, promptly widening the performance bounds to ensure system stability. Once it is determined that the error will not violate the bounds, the system converges asymptotically to zero, thereby guaranteeing the transient and steady-state performance of the system.

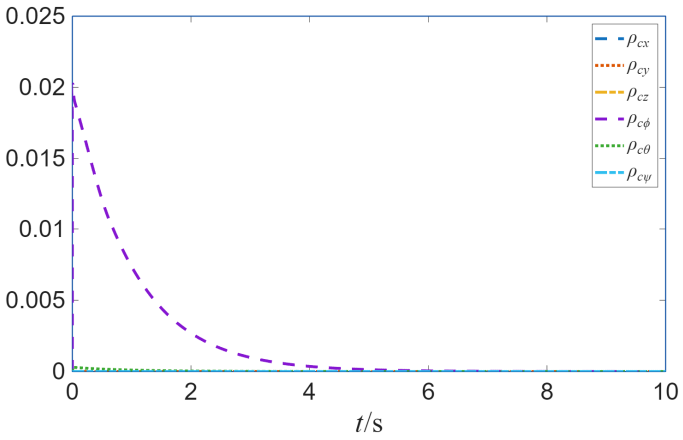

 doi:10.20944/preprints202603.1571.v1

Figure 5. First-order system compensation.

5. Conclusions

This paper proposes a prescribed performance adaptive sliding mode control method to address practical application issues of traditional prescribed performance control and sliding mode control in quadrotor UAV design. Through simulation experiments conducted in Matlab/Simulink, the following conclusions are drawn:

- By defining and stabilizing new error variables, and introducing a first-order compensation system, the issue of traditional prescribed performance functions lacking an adaptive mechanism that dynamically adjusts based on the error state is resolved. This ensures that the error remains within the performance envelope throughout the entire convergence process, thereby enhancing system stability.
- By designing an anti-windup auxiliary system, a non-singular fast terminal backstepping sliding mode controller, and an RBF neural network observer, the proposed method ensures the uniform ultimate boundedness of all system states for the quadrotor subject to time-varying disturbances and input saturation. Furthermore, the calculated error metrics indicate that the system's response performance demonstrates significant improvement compared to traditional methods, with enhanced robustness.
- The proposed piecewise variable-rate reaching law adaptively adjusts controller parameters based on the error state, effectively attenuating chattering and thereby enhancing system stability.

This study contributes to the development of robust control theory for quadrotor UAVs. However, several issues remain to be addressed and further optimization is warranted:

- System uncertainties arising from unknown factors such as rotor failures and time-varying payloads are not considered in this study.
- The inherent chattering phenomenon of sliding mode control has not been fully eliminated.
- The fitting capability of the neural network could potentially be enhanced by incorporating additional hidden layers.
- The real-time performance of the proposed algorithm has not been validated through physical experiments.

Future work could further extend the proposed approach along these directions to enhance both the theoretical innovativeness and engineering practicality, thereby promoting the advancement of UAV technologies.

Author Contributions: Conceptualization, X.L.; methodology, X.L.; software, X.L. and J.J.; validation, X.L.; writing—original draft preparation, X.L.; writing—review and editing, Z.S., H.X. and H.W.;supervision, Z.S., H.X. and H.W. All authors have read and agreed to the published version of the manuscript.

Funding: This work is supported in part by the China Postdoctoral Science Foundation Funded Project GZC20252838 and Natural Science Foundation of Hubei Province 2025AFB390.

Data Availability Statement: Dataset available on request from the authors.

Conflicts of Interest: The authors declare no conflicts of interest.

References

1. Zhou, B.; Gao, F.; Wang, L.; Liu, C.; Shen, S. Robust and Efficient Quadrotor Trajectory Generation for Fast Autonomous Flight. *IEEE Robot. Autom. Lett.* **2019**, *4*, 3529–3536, doi:10.1109/LRA.2019.2927938.
2. Zeng, Y.; Xu, J.; Zhang, R. Energy Minimization for Wireless Communication with Rotary-Wing UAV. *IEEE Trans. Wireless Commun.* **2019**, *18*, 2329–2345, doi:10.1109/TWC.2019.2902559.

 doi:10.20944/preprints202603.1571.v1

3. Luong, N.C.; Hoang, D.T.; Gong, S.; Niyato, D.; Wang, P.; Liang, Y.-C.; Kim, D.I. Applications of Deep Reinforcement Learning in Communications and Networking: A Survey. *IEEE Commun. Surv. Tutorials* **2019**, *21*, 3133–3174, doi:10.1109/COMST.2019.2916583.
4. Zeng, Y.; Wu, Q.; Zhang, R. Accessing from the Sky: A Tutorial on UAV Communications for 5G and Beyond. *Proc. IEEE* **2019**, *107*, 2327–2375, doi:10.1109/JPROC.2019.2952892.
5. Li, B.; Fei, Z.; Zhang, Y. UAV Communications for 5G and beyond: Recent Advances and Future Trends. *IEEE Internet Things J.* **2019**, *6*, 2241–2263, doi:10.1109/JIOT.2018.2887086.
6. Mohsan, S.A.H.; Khan, M.A.; Noor, F.; Ullah, I.; Alsharif, M.H. Towards the Unmanned Aerial Vehicles (UAVs): A Comprehensive Review. *Drones* **2022**, *6*, 147, doi:10.3390/drones6060147.
7. Sishodia, R.P.; Ray, R.L.; Singh, S.K. Applications of Remote Sensing in Precision Agriculture: A Review. *Remote Sensing* **2020**, *12*, 3136, doi:10.3390/rs12193136.
8. Zhou, X.; Wang, Z.; Ye, H.; Xu, C.; Gao, F. EGO-Planner: An ESDF-Free Gradient-Based Local Planner for Quadrotors. *IEEE Robot. Autom. Lett.* **2021**, *6*, 478–485, doi:10.1109/LRA.2020.3047728.
9. Du, H.; Zhu, W.; Wen, G.; Duan, Z.; Lu, J. Distributed Formation Control of Multiple Quadrotor Aircraft Based on Nonsmooth Consensus Algorithms. *IEEE Trans. Cybern.* **2019**, *49*, 342–353, doi:10.1109/TCYB.2017.2777463.
10. Huang, D.; Huang, T.; Qin, N.; Li, Y.; Yang, Y. Finite-Time Control for a UAV System Based on Finite-Time Disturbance Observer. *Aerospace Science and Technology* **2022**, *129*, 107825, doi:10.1016/j.ast.2022.107825.
11. Shao, X.; Sun, G.; Yao, W.; Liu, J.; Wu, L. Adaptive Sliding Mode Control for Quadrotor UAVs with Input Saturation. *IEEE/ASME Trans. Mechatron.* **2022**, *27*, 1498–1509, doi:10.1109/TMECH.2021.3094575.
12. Eliker, K.; Grouni, S.; Tadjine, M.; Zhang, W. Quadcopter Nonsingular Finite-Time Adaptive Robust Saturated Command-Filtered Control System under the Presence of Uncertainties and Input Saturation. *Nonlinear Dyn* **2021**, *104*, 1363–1387, doi:10.1007/s11071-021-06332-3.
13. Chen, G.; Zhang, P.; Wang, Z.; Dong, W. TRP-Controller: An Efficient Anti-Saturation Controller for Quadrotors Performing Yaw-Low-Priority Motions. In Proceedings of the 2021 27th International Conference on Mechatronics and Machine Vision in Practice (M2VIP); IEEE: Shanghai, China, November 26 2021; pp. 310–315.
14. Shao, X.; Zhang, W.; Zhang, W. Improved Prescribed Performance Anti-Disturbance Control for Quadrotors. *Applied Mathematical Modelling* **2021**, *97*, 501–521, doi:10.1016/j.apm.2021.04.010.
15. Koksal, N.; An, H.; Fidan, B. Backstepping-Based Adaptive Control of a Quadrotor UAV with Guaranteed Tracking Performance. *ISA Transactions* **2020**, *105*, 98–110, doi:10.1016/j.isatra.2020.06.006.
16. Shao, X.; Yue, X.; Li, J. Event-Triggered Robust Control for Quadrotors with Preassigned Time Performance Constraints. *Applied Mathematics and Computation* **2021**, *392*, 125667, doi:10.1016/j.amc.2020.125667.
17. Yuan, Y.; Duan, H.; Zeng, Z. Prescribed Performance Evolution Control for Quadrotor Autonomous Shipboard Landing. *IEEE/CAA J. Autom. Sinica* **2024**, *11*, 1151–1162, doi:10.1109/JAS.2024.124254.
18. Zhang, W.; Shao, X.; Zhang, W.; Qi, J.; Li, H. Unknown Input Observer-Based Appointed-Time Funnel Control for Quadrotors. *Aerospace Science and Technology* **2022**, *126*, 107351, doi:10.1016/j.ast.2022.107351.
19. Mofid, O.; Mobayen, S.; Zhang, C.; Esakki, B. Desired Tracking of Delayed Quadrotor UAV under Model Uncertainty and Wind Disturbance Using Adaptive Super-Twisting Terminal Sliding Mode Control. *ISA Transactions* **2022**, *123*, 455–471, doi:10.1016/j.isatra.2021.06.002.
20. Chen, F.; Jiang, R.; Zhang, K.; Jiang, B.; Tao, G. Robust Backstepping Sliding Mode Control and Observer-Based Fault Estimation for a Quadrotor UAV. *IEEE Trans. Ind. Electron.* **2016**, 1–1, doi:10.1109/TIE.2016.2552151.
21. Labbadi, M.; Cherkaoui, M. Robust Adaptive Backstepping Fast Terminal Sliding Mode Controller for Uncertain Quadrotor UAV. *Aerospace Science and Technology* **2019**, *93*, 105306, doi:10.1016/j.ast.2019.105306.
22. Labbadi, M.; Cherkaoui, M. Robust Adaptive Nonsingular Fast Terminal Sliding-Mode Tracking Control for an Uncertain Quadrotor UAV Subjected to Disturbances. *ISA Transactions* **2020**, *99*, 290–304, doi:10.1016/j.isatra.2019.10.012.
23. Liu, K.; Wang, R. Antisaturation Command Filtered Backstepping Control-Based Disturbance Rejection for a Quadarotor UAV. *IEEE Trans. Circuits Syst. II* **2021**, *68*, 3577–3581, doi:10.1109/TCSII.2021.3069967.

 doi:10.20944/preprints202603.1571.v1

24. Zou, Z.; Yang, S.; Zhao, L. Dual-Loop Control and State Prediction Analysis of QUAV Trajectory Tracking Based on Biological Swarm Intelligent Optimization Algorithm. *Sci Rep* **2024**, *14*, 19091, doi:10.1038/s41598-024-69911-5.
25. Wang, J.; Alattas, K.A.; Bouteraa, Y.; Mofid, O.; Mobayen, S. Adaptive Finite-Time Backstepping Control Tracker for Quadrotor UAV with Model Uncertainty and External Disturbance. *Aerospace Science and Technology* **2023**, *133*, 108088, doi:10.1016/j.ast.2022.108088.
26. Zhang, S.; Bi, Y.; Yu, X.; Wu, Y.; Li, C. Adaptive RBFNN-Based Fault-Tolerant Control for Robotic Manipulators with Prescribed Performance. *Neurocomputing* **2025**, *647*, 130322, doi:10.1016/j.neucom.2025.130322.